JOURNAL OF AIRCRAFT
Vol. 35, No. 2, March–April 1998

Effect of Wake Structure on Blade–Vortex Interaction Phenomena: Acoustic Prediction and Validation

Judith M. Gallman*
NASA Ames Research Center, Moffett Field, California 94035-1000
Klaus-J. Schultz†
DLR, German Aerospace Research Establishment, Braunschweig, Germany
Pierre Spiegel‡
ONERA, Chatillon 92320, France
and
Casey L. Burley§
NASA Langley Research Center, Hampton, Virginia 23681-0001

The higher harmonic control aeroacoustic rotor test conducted at Duits-Nederlandse Wind Tunnel has made extensive measurements of the rotor aerodynamics, far-field acoustics, wake geometry, and the blade motion for powered descent flight conditions. These measurements have been used to validate and improve the prediction of blade–vortex interaction (BVI) noise. The improvements made to the BVI modeling after the evaluation of the test data are discussed. The effect of these improvements on the acoustic-pressure predictions is shown. These improvements include restructuring the wake, modifying the core size, incorporating the measured blade motion into the calculations, and attempting to improve the dynamic blade response. A comparison of four different implementations of the Ffowcs Williams and Hawkings equation is presented. A common set of aerodynamic input has been used for this comparison.

Introduction

TO correctly predict the aerodynamic and acoustic pressure for a helicopter operating in powered descent flight, it is of utmost importance to correctly model the wake geometry of the vortices shed from the rotor tips. The wake-geometry model should contain information on the vortex location, strength, and core size. A recent international cooperative test, the higher harmonic control aeroacoustic rotor test (HART), has made extensive measurements of the rotor aerodynamics, far-field acoustics, wake geometry, and blade motions.[1] In preparation for this test, an international team of researchers from DLR, Germany, ONERA, France, the US Army Aeroflightdynamics Directorate (AFDD), and NASA Langley Research Center (LaRC) have been improving the prediction capability of blade-vortex interaction (BVI) phenomena. This prediction capability includes models of the vortex geometry, aeroelastic blade motion, aerodynamic surface pressure, and far-field acoustic predictions.

The first validation effort of the prediction team was documented in Ref. 2. This validation effort included wake-geometry predictions, aerodynamic surface pressure predictions, and acoustic far-field predictions of the two-bladed, one-seventh-scale model operation load survey (OLS) rotor tested in the Duits-Nederlandse Wind Tunnel (DNW) in 1982.[3,4] Leading-edge pressure transducers at $x/c = 0.03$ and far-field acoustic data from this test were used for the validation efforts. The prediction codes compared reasonably well with the test data and captured the qualitative characteristics of the acoustic test data; however, further improvements to the wake-geometry models were necessary to adequately predict the quantitative characteristics of the acoustic pressure needed to evaluate noise-reduction techniques.

The second validation effort of the HART prediction team focused on the prediction of the wake geometry, aeroelastic blade motion, aerodynamic surface pressure, and far-field acoustics for the dynamically scaled, four-bladed, 40% model of the bearingless BO-105 main rotor.[5] The predictions are documented in Ref. 6. Unfortunately, only the far-field acoustic pressures were available for this validation effort. Therefore, the wake geometry and the aeroelastic and aerodynamic predictions of each prediction team member were compared to one another to provide a better understanding of how each method predicted the blade–vortex interaction (BVI) phenomena. This exercise proved the importance of including the aeroelastic effects in the prediction of BVI noise; however, the most important conclusion of this exercise was that the prediction team was capable of modeling the effect of 4/rev higher harmonic control (HHC) on BVI noise for the BO-105 model rotor.

The acoustic predictions of the third validation effort are documented in the current paper. The third validation effort is focused on predicting the test points run during the HART program. The blades used for this test are the same BO-105 model scale blades used for the European HELINOISE aeroacoustic rotor test.[7] Both the pretest and the posttest acoustic predictions are presented. The pre-HART acoustic predictions are shown to indicate the status of the prediction ability before the HART data were available to help the prediction team improve their BVI phenomena modeling capability. The pre-HART predictions were done to help define the test matrix, improve the measurement techniques, and provide background for possible unexpected experimental results. A brief summary

Presented as Paper 95-022 at the AIAA/CEAS 1st Joint Aeroacoustics Conference, Munich, Germany, June 12–15, 1995; received Nov. 20, 1995; revision received Oct. 27, 1997; accepted for publication Oct. 30, 1997.

*Research Scientist, U.S. Army Aeroflightdynamics Directorate, ATCOM; currently Senior Specialist Engineer, Propulsion Analysis and IR&D, Boeing Commercial Airplane Group, Wichita Division, Wichita, KS 67209. Member AIAA.

†Research Scientist, Institut für Entwurfsaerodynamik.

‡Research Scientist, Acoustics Division, 29 avenue de la Division Leclerc.

§Research Scientist, Acoustics Division. Senior Member AIAA.

of the improvements made to the BVI modeling will also be included. For more information on the details of the improvements to the BVI modeling, see Ref. 8.

All of the prediction team members use a numerical simulation of the Ffowcs Williams and Hawkings (FW–H) equation[9] to predict the acoustics. Therefore, all predictions require detailed information about the aerodynamic surface pressure on the rotor blade. The aerodynamic surface pressure calculations for the acoustic results shown in this paper are documented in Ref. 8. To directly compare the different implementations of the FW–H equation of each team member, a common set of blade surface pressures was used by all team members. These comparisons document any differences in acoustic predictions resulting from different implementations of the FW–H equation.

Acoustic Prediction Codes

For the acoustic calculations, the DLR has developed the acoustic code AKUROT,[10] ONERA computes the acoustics using the PARIS code,[11] AFDD utilizes the RAPP code,[12] and NASA LaRC runs WOPWOP[13] to predict the acoustics. All of the acoustic prediction codes use only the linear thickness and loading terms of the FW–H equation, assuming that the noise from the nonlinear quadruple term is negligible for the BVIs studied in this program.

DLR Acoustic Prediction Methodology

To predict the acoustic pressure, the DLR uses the acoustic code AKUROT. This code was developed in 1987[4] and first validated with experimental data from the 1982 AH1–OLS model rotor test in the DNW. The code is based on the FW–H equation (Farassat formulation 1, in which the spatial derivative of the force integral can be converted to a time derivative; see Ref. 13 for detailed discussion), and includes a thickness noise term and a loading noise term for the HART calculations.

The input data for the loading term are provided by the S4 rotor simulation code.[6] Because the aerodynamic model in the S4 code is based on lifting-line theory, loading data are available only at the quarter chord line at 20 radial stations and 180 azimuthal stations. For use in the acoustic prediction code, the loading data were interpolated to get inputs for 1024 azimuthal and 160 radial stations. The acoustic code uses a chordwise compact model of the loading noise.

NASA LaRC Acoustic Prediction Methodology

NASA LaRC uses the rotor acoustic code WOPWOP,[13] which implements the acoustic formulation 1A of Farassat (the time derivatives to be taken inside the acoustic pressure integral) to predict the acoustic pressure. This time-domain representation of the FW–H equation does not include the quadrapole term for supersonic flow. The input to WOPWOP includes the physical characteristic of the rotor blade and the aerodynamic blade loading as a function of azimuthal position. For the predictions presented, the loads were input to WOPWOP every 1 deg of azimuth. When the aerodynamic input used in WOPWOP is calculated by HIRES,[14] the loading noise is modeled by a chordwise compact source. When a chordwise distribution of the blade loading is available, the loading noise is modeled by noncompact sources distributed over the chord.

ONERA Acoustic Prediction Methodology

At ONERA the noise radiation is computed by the PARIS code.[11] PARIS is based on the FW–H equation and uses a time-domain formulation that predicts the loading and thickness noise. The loading noise is computed using a pressure distribution provided by AHRIS.[15] An efficient spanwise interpolation model of the airloads has been implemented in PARIS to minimize the amount of airload data required for BVI noise predictions. This interpolation method identifies the BVI impulsive events in the airloads generated at each individual blade section and accounts for the phase and amplitude. This method, used with aerodynamic inputs from 11 blade sections, provides the same result as a prediction using airload data from 30 sections without interpolation.

AFDD Acoustic Prediction Methodology

At AFDD, RAPP,[12] a rotor acoustic prediction program based on the FW–H equation, calculates the acoustic pressure using the full potential rotor (FPR)[16–19] computed surface pressures. RAPP can use either the chordwise compact or noncompact formulation. When the force terms in the FW–H equation are modeled as chordwise compact sources, the sources are distributed spanwise along the quarter chord of the acoustic planform. The acoustic planform consists of the locations of the contributing sources. This method is referred to as the acoustic lifting-line method.

When the noncompact formulation is used to model the force terms, 20 sources are distributed over the airfoil surface at each spanwise location. For both formulations, 11 spanwise stations, distributed over the outer 60% of the span, are used in the computation. The time step for the acoustic calculation is 0.7 deg. The time resolution of the input aerodynamic loading is 0.125 deg. The advantage of the compact formulation as compared with the noncompact formulation is the reduced time and memory required. For the compact formulation, only the section loading is needed at each spanwise location for each time step (0.125 deg), whereas for the noncompact formulation the pressure at the 20 surface points is needed at each spanwise station for each time step.

Test and Model Description

The HHC aeroacoustic rotor test configuration consisted of a Mach scaled, 40% model of the hingeless BO-105 main rotor mounted on the DLR test rig. The rectangular rotor blades have −8 deg of linear twist, a radius of 2 m, a constant chord of 0.121 m, and a modified NACA 23012 airfoil. The model is highly instrumented with 124 pressure transducers and 53 strain gauges. The test was run in the 6 m × 8 m open-jet configuration of the DNW. The acoustic measurements were made with an array of 11 microphones mounted on a ground-based traverse mechanism. The microphones are arranged symmetrically with respect to the rotor hub and are spaced 0.54 m apart. The traverse, located 2.3 m below the hub of the rotor, travels from 4 m upstream of the rotor hub to 4 m downstream of the rotor hub. Data are acquired while the microphone array is continuously traversing downstream, but the actual measurement locations are at 0.5-m intervals starting at 4.0 m upstream of the hub, resulting in 187 measurement locations below the rotor hub. Figure 1 shows the resulting grid of measurement locations with respect to the rotor plane. One acoustic microphone was located on the body of the test rig and two acoustic microphones were mounted in the plane of the rotor on the 8 m × 6 m nozzle. For each test condition, the acoustic pressure was recorded for 30 rotor revolutions at a rate of 2048 data points per revolution. The pressure time histories and sound-pressure levels presented in this paper for code validation are based on the average of 30 revolutions.

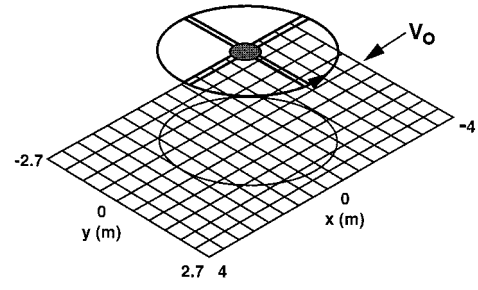

Fig. 1 Grid of 187 microphone locations below the rotor plane.

Table 1 Test points used for code validation

Run number	C_T	μ	α_s, deg	RPM	HHC amp, deg	HHC phase, deg
Baseline (run 140)	0.00432	0.152	5.3	1041	0.0	0.0
Low noise (run 138)	0.00413	0.152	5.3	1041	0.87	296
Low vibration (run 133)	0.0044	0.151	5.3	1041	0.83	177

Table 2 Microphone positions for maximum SPL

	Advancing side, m			Retreating side, m		
Run number	x	y	z	x	y	z
Baseline (run 140)	0.0	2.18	−2.29	2.0	−1.07	−2.28
Low noise (run 138)	−0.5	1.1	−2.29	2.0	−1.07	−2.28
Low vibration (run 133)	0.05	2.18	−2.29	2.5	−1.07	−2.28

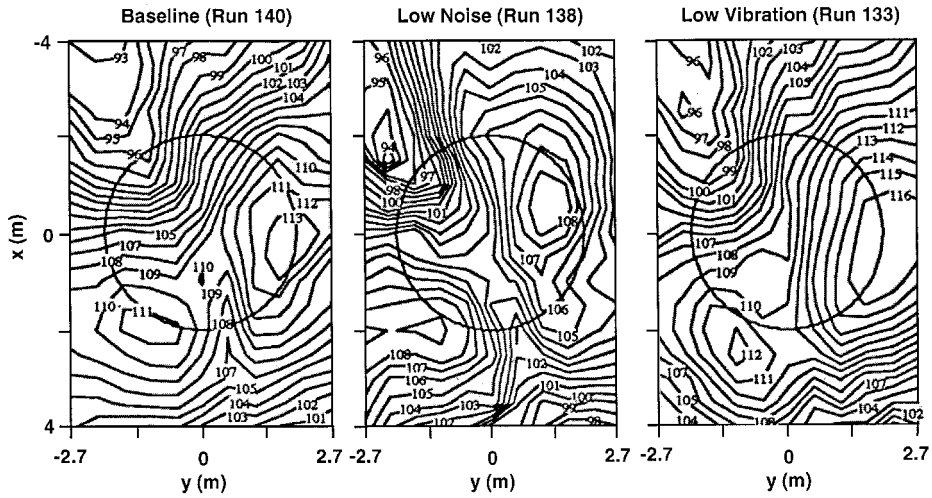

Fig. 2 Measured midfrequency (6th–40th harmonic) SPL contour plots for the test cases listed in Table 1.

The HART test matrix consisted of descent flight conditions with a variation of the glide path angle from −3 deg to +12 deg and a variation in the advance ratio from 0.144 to 0.275. The nominal test condition, or the baseline case, simulated a landing approach with a glide path angle of 6 deg and an advance ratio of 0.15. This case corresponds to a shaft tilt angle of 5.3 deg and a wind-tunnel velocity of 33 m/s. For this baseline condition, a systematic variation in phase shift of the HHC was performed for 3, 4, and 5/rev input of 0.8-deg amplitude. The most effective HHC input for reducing noise and vibration was the 3/rev. Therefore, the measured data and the analytic solutions presented in this paper for code validation will be the baseline case and two cases with 3/rev HHC input of 0.8 deg. One case corresponds to low noise and one case corresponds to low vibration. The test conditions presented in this paper are listed in Table 1.

Results

For the test cases listed in Table 1, the measured and predicted acoustic-pressure time histories are presented at the location of maximum sound pressure level (SPL) on the retreating side and on the advancing side of the rotor. The locations of maximum SPL, determined from the measured midfrequency SPL, are different for each test condition and are listed in Table 2. The average time history at each measurement point below the rotor (see Fig. 1) is used to determine the midfrequency SPL. The band limit is the 6th to the 40th blade passage frequency. This midfrequency band is believed to contain the frequencies present in BVI noise. The measured midfrequency SPL contour plots for the three test cases listed in Table 1 are shown in Fig. 2. The measured acoustic–pressure time histories are shown in Fig. 3.

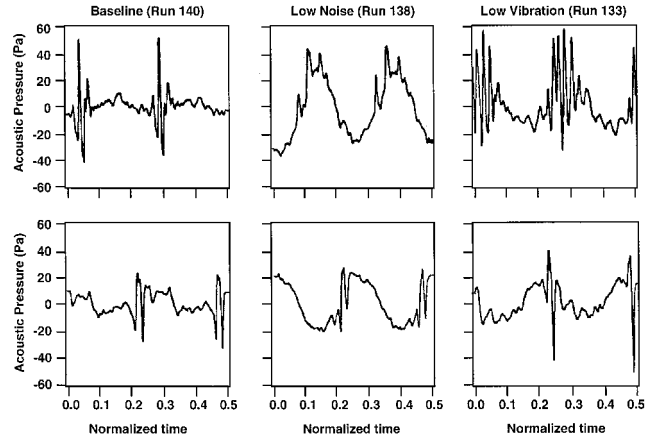

Fig. 3 Measured acoustic–pressure time histories for the test cases listed in Table 1. Row 1: advancing side microphone locations listed in Table 2. Row 2: retreating side microphone locations listed in Table 2.

DLR Pre-HART and Post-HART Acoustic Predictions

The pre-HART acoustic predictions made by the DLR are based on the method described in Ref. 6. In this method, the S4 rotor simulation code predicts the spanwise blade loading needed by the acoustic code AKUROT to predict the acoustic pressure. For the post-HART acoustic predictions, the wake model in S4 has been modified. The modification to the wake model is mainly an application of a wake contraction model. A 15% contraction has been applied to the baseline case, and low-noise case and a 10% contraction has been applied to the

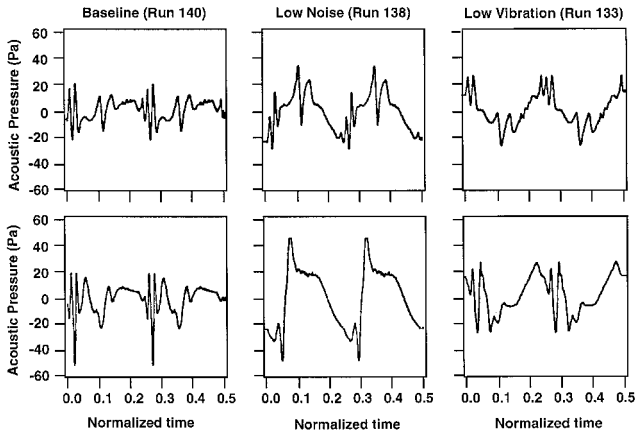

Fig. 4 DLR-predicted acoustic–pressure time histories for the advancing side microphone locations listed in Table 2. Row 1: pretest predictions. Row 2: posttest predictions.

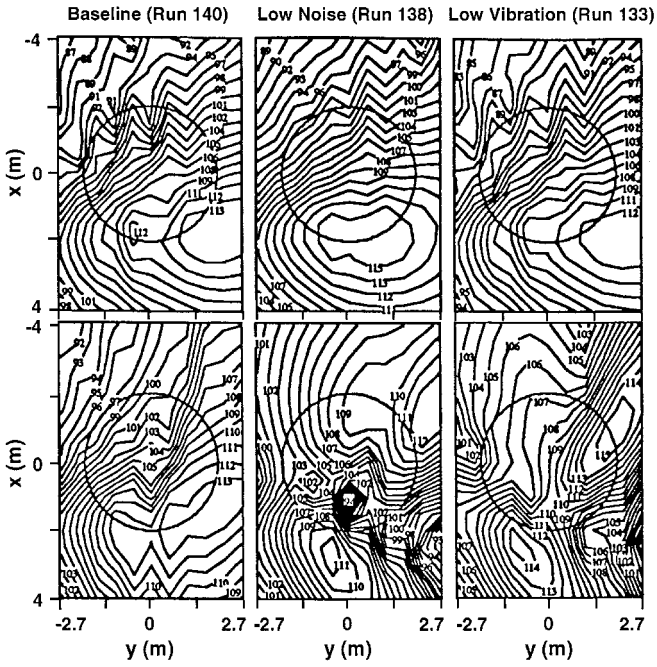

Fig. 5 DLR-predicted midfrequency SPL contours. Row 1: pretest predictions. Row 2: posttest predictions.

low-vibration case. Also, the vortex core radius was redefined to be equal to the vortex core measured during the HART program. In an attempt to determine the effect of wake geometry on the aeroacoustic predictions for the two cases with HHC, the orientation of the wake with respect to the tip path plane was adjusted so that the miss distance between the blade and the vortex would be similar to the measurements made of the miss distance during the HART program. In addition, for the low-vibration case, a double vortex structure was used as measured during the HART test. The predicted acoustic–pressure time histories for the three test cases at the advancing side microphone locations listed in Table 2 are shown in Fig. 4. The top row contains the pretest predictions and the bottom row contains the posttest predictions. For the baseline case, the wake restructuring improves the peak-to-peak levels of the waveform on the advancing side. Not only is the peak-to-peak level improved on the advancing side for the low-noise case, but the overall waveform compares better to the measured data. The changes to the waveforms because of the wake restructuring are not necessarily positive for the low-vibration case. Perhaps the wake restructuring needs to be optimized for each test case. The contour plots of the midfrequency SPLs for the three test cases are shown in Fig. 5. The contour plots in the first row are the pre-HART predictions and the contour plots in the second row are the post-HART predictions. The wake restructuring only slightly affects the contour plots for the baseline and the low-noise cases; however, it improves both the magnitude and the directivity characteristics of the low-vibration case.

NASA LaRC Pre-HART and Post-HART Acoustic Predictions

The methodology used for pre-HART acoustic predictions made by NASA LaRC is also discussed in detail in Ref. 6. The prediction method begins with a 10-deg azimuthal resolution of the rotor wake calculated by CAMRAD.MOD1. HIRES then computes the airloads at 1-deg azimuthal increments and at 75 radial stations. The rotor blade dynamics are calculated by CAMRAD.MOD1. For the post-HART predictions, the measured blade dynamics are used to prescribe the blade motion in CAMRAD.MOD1 before the HIRES computation of the airloads. The NASA LaRC-predicted acoustic–pressure time histories at the advancing side microphone locations for the three test cases are shown in Fig. 6. The time histories in the top row are the pretest predictions and the time histories in the bottom row are the posttest predictions. The

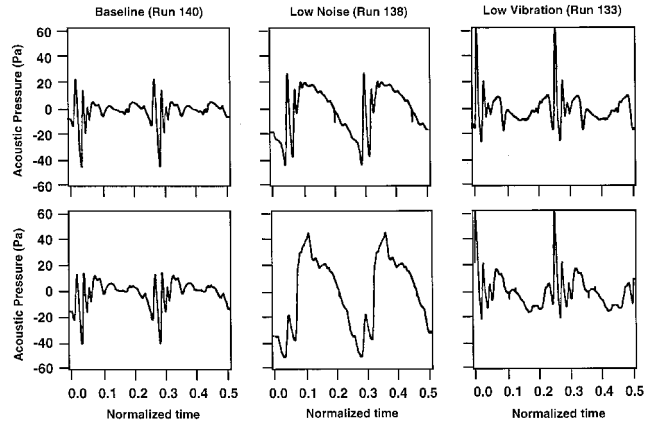

Fig. 6 NASA LaRC-predicted acoustic–pressure time histories for the advancing side microphone locations listed in Table 2. Row 1: pretest predictions. Row 2: posttest predictions.

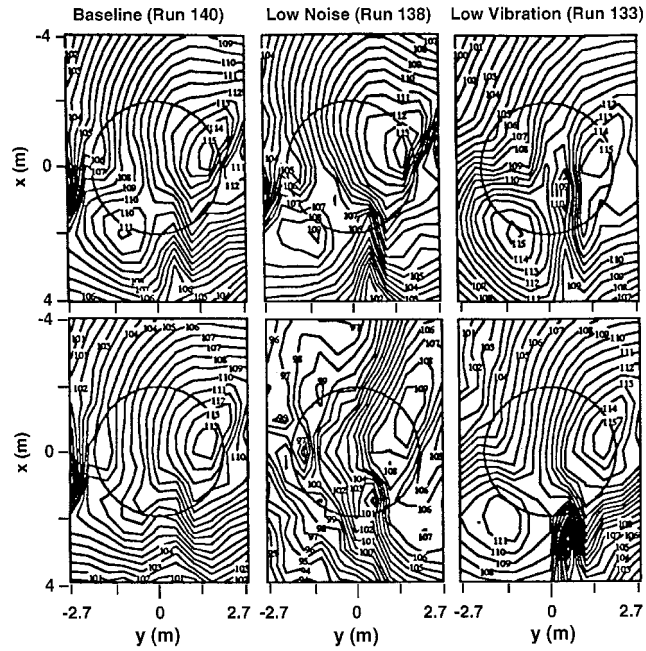

Fig. 7 NASA LaRC-predicted midfrequency SPL contours. Row 1: pretest predictions. Row 2: posttest predictions.

peak-to-peak levels are reduced on the retreating side of the rotor for the baseline case, but the waveform does not change when the measured blade dynamics are used for the prediction. For the low-noise case, the low-frequency character of the waveform is increased and the peak-to-peak levels are decreased by the application of the measured blade dynamics. The low-vibration case is similar to the baseline case, wherein the peak-to-peak levels are reduced on the retreating side without much change to the waveform when the predicted blade dynamics are replaced by the measured blade dynamics in the prediction of the airloads. The pretest and posttest NASA LaRC-predicted contour plots of the midfrequency SPLs are shown in Fig. 7. For the baseline case, the SPLs are reduced in the posttest calculations. Also, the local peak on the retreating side has been eliminated. The elimination of the local peak in the posttest prediction is also evident for the low-noise case. For this case, the levels over the whole contour have been decreased. The low-vibration case changes only slightly by the application of the measured blade motion to the airloads prediction. The peak levels on the retreating side are reduced without the elimination of the retreating side local maximum.

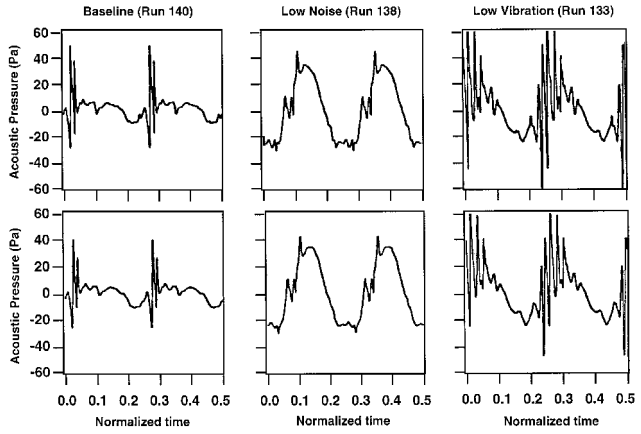

Fig. 8 ONERA-predicted acoustic–pressure time histories for the advancing side microphone locations listed in Table 2. Row 1: pretest predictions. Row 2: posttest predictions.

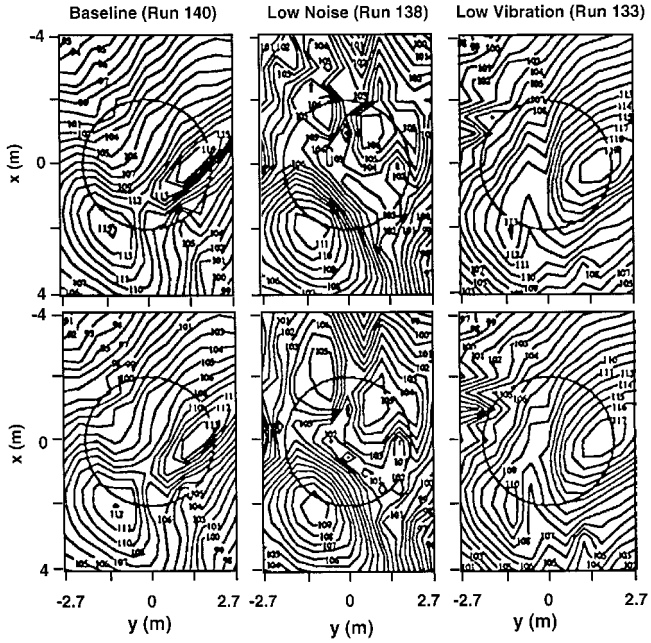

Fig. 9 ONERA-predicted midfrequency SPL contours. Row 1: pretest predictions. Row 2: posttest predictions.

ONERA Pre-HART and Post-HART Acoustic Predictions

The difference between the pre-HART and the post-HART predictions made by ONERA is a change in the wake model in the aerodynamic analysis code AHRIS. A detailed description of the pretest ONERA prediction methodology can be found in Ref. 6. The pretest AHRIS wake model used a vortex core radius evolution law based on extrapolated hot-wire measurements of a two-bladed rotor model in hover.[20] The viscous core radii obtained with this law are often smaller than 0.1 chord on the advancing side and approximately 0.15 on the retreating side. The posttest AHRIS wake model uses an improved evolution law based on the preliminary analysis of the HART laser Doppler velocimetry measurements. The adjusted law results in viscous core radii of 0.25 chord on the retreating side that are in agreement with the experimental data. The viscous core radii on the advancing side changes only slightly. The ONERA-predicted acoustic–pressure time histories of the three test cases are shown in Fig. 8 for the advancing side microphone locations. The time histories in the top row are the pretest predictions and the time histories in the bottom row are the posttest predictions. The only difference between the pre-HART and the post-HART acoustic–pressure time histories for all three test cases is the magnitude of the

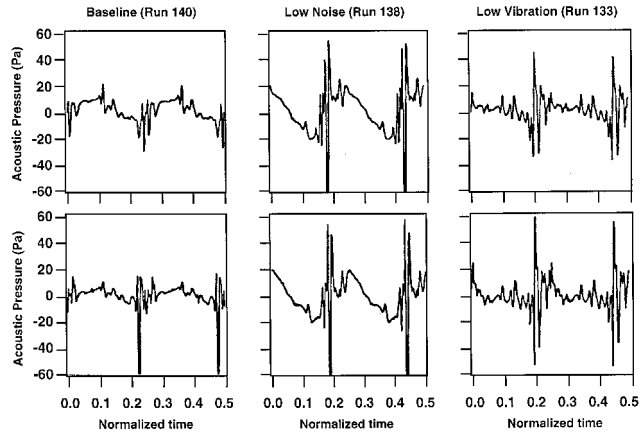

Fig. 10 AFDD-predicted acoustic–pressure time histories for the advancing side microphone locations listed in Table 2. Row 1: pretest predictions. Row 2: posttest predictions.

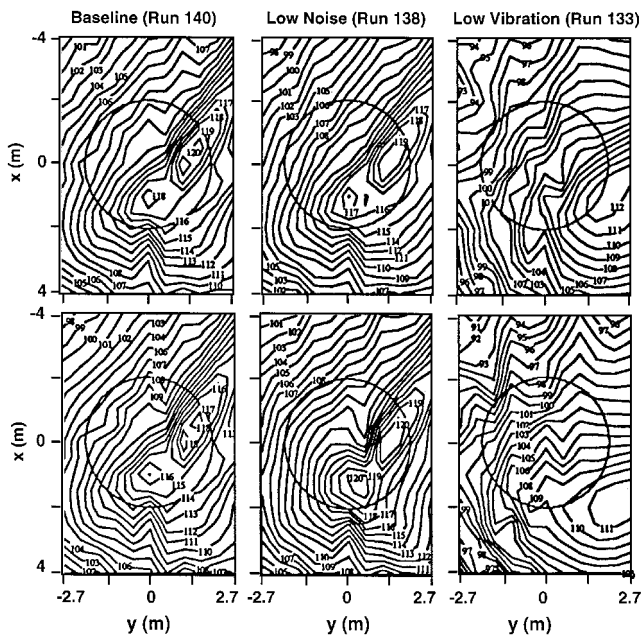

Fig. 11 AFDD-predicted midfrequency SPL contours. Row 1: pretest predictions. Row 2: posttest predictions.

peaks. This is the expected result of increasing the core radius in the airloads computation. The ONERA-predicted pretest and posttest midfrequency SPLs are shown in Fig. 9. The only difference between the pretest and posttest SPL contours is the lower levels for the posttest predictions.

AFDD Pre-HART and Post-HART Acoustic Predictions

The main differences between the pre-HART predictions and the post-HART predictions made by AFDD are a change to the partial angle calculation and the fine-tuning of the dynamic model of the rotor blade in an attempt to improve the dynamic blade motion. The AFDD pre-HART prediction methodology is summarized in Ref. 6. A closer look at the partial angles calculated by CAMRAD/JA revealed that the angles were not being calculated correctly. CAMRAD/JA computes the partial angles by subtracting the induced velocity caused by the tip vortices within the computational domain of FPR from the inflow angles. Specifying a core radius of 2.0 chords for the partial angle calculation eliminates the anomalies from the partial angle calculation. A core radius of 0.20 chord is used for all other CAMRAD/JA and FPR calculations. The AFDD-predicted acoustic–pressure time histories of the three test cases are shown in Fig. 10 for the advancing side microphone locations. The time histories in the top row are the pretest predictions and the time histories in the bottom row are the posttest predictions. There is only a slight change in magnitude between the pretest and posttest predictions without much change in waveform for both the advancing and retreating side microphone locations. The AFDD-predicted midfrequency SPL contours are shown in Fig. 11. There is little difference between the pretest and posttest prediction of the SPLs for the baseline case. The slight decrease in contour levels for this case is most likely caused by the change in the partial angles. The contour levels for the low-noise case actually increase for the post-HART predictions with only a slight change in directivity. The actual contour levels for the low-vibration case change only slightly, but the local maximum on the advancing side has moved aft for the posttest predictions.

Acoustic Predictions Using Common Aerodynamic Input

Even though all of the prediction team members use a numerical simulation of the FW–H equation, each implementation is different. To determine whether there are any differences in the acoustic predictions caused by the specific implementations of the FW–H equation, all of the prediction team members use a common set of aerodynamic blade surface

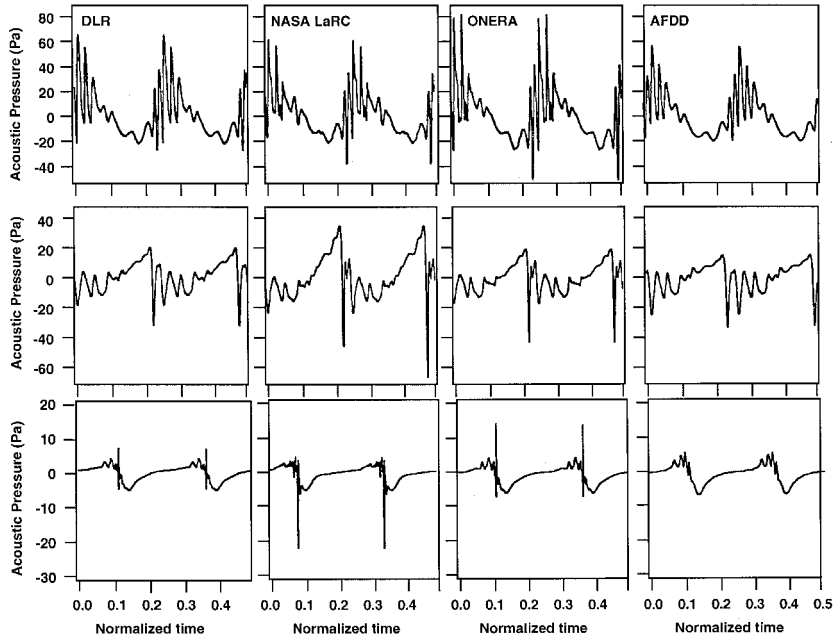

Fig. 12 Predicted acoustic–pressure time histories using a common set of aerodynamic input for Run 133. Row 1: advancing side microphone location listed in Table 2 for run 133. Row 2: retreating side microphone location listed in Table 2 for run 133. Row 3: in-plane microphone location.

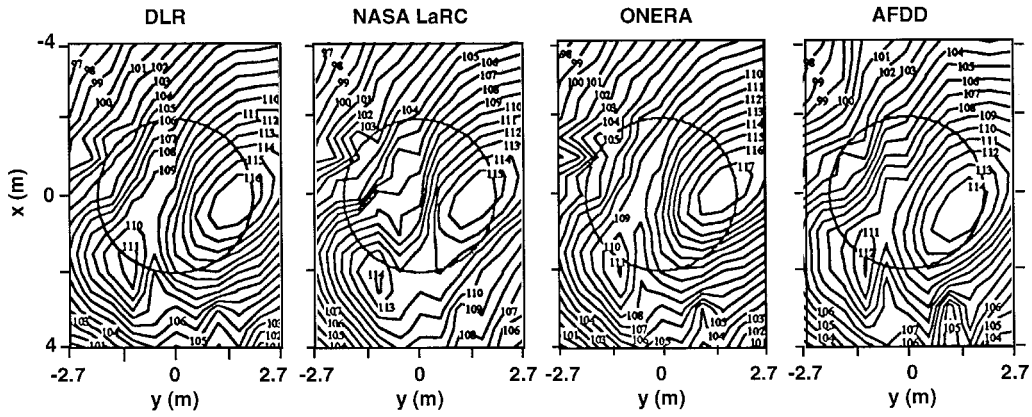

Fig. 13 Predicted midfrequency SPL contours for run 133 using a common set of aerodynamic input.

pressures. The common set is a prediction of the low-vibration case (run 133) provided by ONERA. Each team member used the blade loading at the same 30 radial stations and 41 chordwise positions provided by ONERA for the noncompact model of the dipole source. All acoustic predictions for this case were made assuming that the rotor was stiff, i.e., no flapping, bending, or torsion. The measured cyclic and collective pitch was used to determine the blade attitude. Also, the uncorrected shaft angle was used to define the location of the blade with respect to the observer. The resulting predicted acoustic–pressure time histories are shown in Fig. 12. The predictions in the first row in Fig. 12 are for a microphone located on the advancing side of the rotor, and the predictions in the second row are for a microphone located on the retreating side of the rotor. These microphone locations are listed in Table 2 for run 133. The predictions in the third row are for a microphone located in the plane of the rotor. This microphone is mounted on the nozzle and is at $x = -6.71$ m, $y = 3.395$ m, and $z = 0.0$. There are only a few slight differences in magnitude for the acoustic predictions at the advancing side microphone. The differences in magnitude are much greater for the predictions at the retreating side microphone. For the predictions at the in-plane microphone, the main difference is the magnitude of the spike and the fact that it is not evident in the AFDD predictions. The predicted midfrequency SPL contours are shown in Fig. 13. The character of the directivity pattern is quite similar for all four methods. NASA LaRC predicts higher levels downstream of the rotor than do the rest of the prediction team, and the local maximum on the advancing side is slightly higher for the ONERA predictions.

Summary and Conclusions

The pretest and posttest acoustic predictions for the higher harmonic control aeroacoustic rotor test have been presented. The comparisons between the pretest and posttest predictions indicate how the HART program can guide researchers to improve the aeroacoustic and dynamic modeling of the BVI phenomena so that low-noise concepts such as HHC can be explored. To improve their prediction capability, the DLR combined a contraction of their prescribed wake model with a reorientation of the wake geometry with respect to the tip path plane. This combined restructuring of the wake can improve the aeroacoustic predictions and will be used to refine the DLR free-wake model. The substitution of the measured blade dynamics for the predicted dynamics does improve the aeroacoustic predictions made by NASA LaRC. This example demonstrates the necessity of properly calculating the blade motion for BVI noise predictions, especially for cases with HHC input. ONERA's posttest predictions show that changing the core size of the tip vortices to more closely agree with the measured core sizes only slightly affects the magnitude of the predicted acoustic–pressure time histories and the SPL contours. AFDD's fine-tuning of the dynamic model of the rotor blade affected the aeroacoustic predictions only slightly. The prediction of the dynamic blade motion by CAMRAD/JA is still not adequate for the cases with HHC input.

There are small but distinct differences in the acoustic predictions made by each of the prediction team members when the same aerodynamic input is used. The exact cause of these differences is not currently obvious, but documenting the extent of the differences should help the rotorcraft community understand where the state of the art lies in acoustic prediction methodology.

Acknowledgments

We acknowledge the following colleagues who contributed to this paper: Chee Tung of AFDD, Wolf Splettstoesser and Heino Buchholz of DLR, and Thomas F. Brooks and D. Douglas Boyd Jr. of NASA.

References

[1]Yu, Y. H., Gmelin, B., Heller, H., Phillipe, J. J., Mercker, E., and Preisser, J. S., "HHC Aeroacoustics Rotor Test at the DNW—The Joint German/French/US HART Project," 20th European Rotorcraft Forum, Amsterdam, The Netherlands, Oct. 1994.

[2]Yu, Y. H., Tung, C., Gallman, J. M., Splettstoesser, W. R., Schultz, K. J., Van der Wall, B., Spiegel, P., and Rahier, G., "Aerodynamics and Acoustics of Rotor Blade–Vortex Interactions: Analysis Capability and Its Validation," AIAA Paper 93-4332, Oct. 1993.

[3]Boxwell, D. A., Schmitz, F. H., Splettstoesser, W. R., and Schultz, K. J, "Model Helicopter Rotor High-Speed Impulsive Noise: Measured Acoustics and Blade Pressures," 9th European Rotorcraft Forum, Stresa, Italy, Sept. 1983.

[4]Boxwell, D. A., Schmitz, F. H., Splettstoesser, W. R., and Schultz, K. J., "Helicopter Model Rotor-Blade Vortex Interaction Impulsive Noise: Scalability and Parametric Variations," *Journal of the American Helicopter Society*, Vol. 32, No. 1, 1987, pp. 3–12.

[5]Splettstoesser, W. R., Schultz, K. J., Kube, R., Brooks, T. F., Booth, E. R., Niesl, G., and Streby, O., "BVI Impulsive Noise Reduction by Higher Harmonic Pitch Control: Results of a Scaled Model Rotor Experiment in the DNW," 17th European Rotorcraft Forum, Berlin, Germany, Sept. 1991.

[6]Beaumier, P., Demargne, A., Prieur, J., Rahier, G., Spiegel, P., Kube, R., Van der Wall, B. G., Schultz, K. J., Splettstoesser, W. R., Tung, C., Gallman, J. M., Yu, Y. H., Brooks, T. F., Burley, C. L., and Boyd, D. D., "Aerodynamic and Acoustic Effect of Higher Harmonic Control on Helicopter Rotor Blade–Vortex Interaction: Predictions and Preliminary Validations," 75th Fluid Dynamics Panel Meeting and Symposium on Aerodynamics and Aeroacoustics of Rotorcraft, AGARD, Berlin, Germany, Oct. 1994.

[7]Splettstoesser, W. R., Niesl, G., Cenedese, F., Nittie, F., and Papanikas, D. G., "Experimental Results of the European HELINOISE Aeroacoustic Rotor Test in the DNW," *Proceedings of the 19th European Rotorcraft Forum*, St. Petersburg, Russia, 1993.

[8]Tung, C., Gallman, J. M., Kube, R., Wagner, W., Van der Wall, B., Brooks, T. F., Burley, C. L., Beaumier, P., and Rahier, G., "Prediction and Measurement of Blade–Vortex-Interaction Loading," CEAS/AIAA Aeroacoustic Conf., Munich, Germany, June 1995.

[9]Ffowcs Williams, J. E., and Hawkings, D. L., "Sound Generation by Turbulence and Surfaces in Arbitrary Motion," *Philosophical Transactions of the Royal Society of London*, Series A, Vol. 264, No. 1151, 1969, pp. 321–342.

[10]Schultz, K. J., and Splettstoesser, W. R., "Prediction of Helicopter Impulsive Noise Using Measured Blade Pressures," 43rd Annual Forum of the American Helicopter Society, St. Louis, MO, May 1993.

[11]Spiegel, P., Rahier, G., and Michea, B., "Blade–Vortex Interaction Noise: Prediction and Comparison with Flight and Windtunnel Tests," 18th European Rotorcraft Forum, Avignon, France, Sept. 1992.

[12]Gallman, J. M., "The Validation and Application of a Rotor Acoustic Prediction Computer Program," *Proceedings of the 13th Army Science Conference*, Army Science Board, Durham, NC, 1990.

[13]Brentner, K. S., "Prediction of Helicopter Rotor Discrete Frequency Noise," NASA TM-87721, Oct. 1986.

[14]Brooks, T. F., Booth, E. R., Jr., Splettstoesser, W. R., Kube, R., Niesl, G., and Steby, O., "HHC Study in the DNW to Reduce BVI Noise—An Analysis," AHS-RAes International Technical Specialists Meeting on Rotor Acoustics and Rotor Fluid Dynamics, Philadelphia, PA, Oct. 1991.

[15]Rahier, G., and Spiegel, P., "Bruit d'Interaction Pale-Tourbillon d'un Rotor Principal d'Hélicoptère," *Journal d'Acoustique*, Vol. 5, May 1992, pp. 171–180.

[16]Strawn, R., and Tung, C., "The Prediction of Transonic Loading on Advancing Helicopter Rotors," NASA TM-88238, USAVSCOM TM-886-A-1, April 1986.

[17]Strawn, R. C., and Caradonna, F. X., "Conservative Full-Potential Model for Unsteady Transonic Rotor Flows," *AIAA Journal*, Vol. 25, No. 2, 1987, pp. 193–198.

[18]Caradonna, F. X., and Strawn, R. C., "An Experimental and Computational Study of Rotor-Vortex Interaction," *Vertica*, Vol. 12, No. 4, 1988, pp. 314–327.

[19]Gallman, J. M., Tung, C., Yu, Y. H., and Low, S. L., "Prediction of Blade–Vortex Interaction Noise with Applications to Higher Harmonic Control," AIAA Paper 93-4331, Oct. 1993.

[20]Plantin de Hugues, P., "Etude du System Tourbillonnaire Genere en Extremite de Pale d'un Rotor d'Helicoptere en Vol Stationanaire," M.S. Thesis, Univ. of Aix-Marseille II, Marseille, France, 1991.